JurnalTribologi 42 (2024) 198-215

Jurnal Tribologi
Website : jurnaltribologi.mytribos.org e-issn: 2289-7232

Cavitation modeling effect on tribological performances in piston skirt lubrication

Feghoul El Hadj Mohamed [1*], Belalia Azeddine [1], Aboshighiba Hicham [2], Tahar Abbes Miloud [1]

[1] Laboratory of Mechanical and Energy, University of Hassiba Benbouali, ALGERIA.
[2] University of Ibn Khaldoun, ALGERIA.
[*]Corresponding author: e.feghoul@univ-chlef.dz

KEYWORDS

Piston skirt
Lubrication
Cavitation
Murty algorithm
Tribology

ABSTRACT

Cavitation is a major concern for hydrodynamic lubrication of mechanical components toward detrimental phenomena related to cavitation such as noise, vibration and wear by erosion. For this purpose, this study focuses on a comparison between the effect of cavitation and no cavitation in piston lubrication in order to show the importance of cavitation effect on the secondary movement of the piston and the tribological parameters. The non considering cavitation is handled by the classical Reynolds model, the considering cavitation is handled by the JFO model modified by Elrod. To determine the cavitation zone, we employ the Murty algorithm. The results show that taking cavitation into account in the hydrodynamic piston lubrication model gives consistency between the hydrodynamic pressure distribution, the secondary movement and subsequently the minimum film thickness, friction and friction power loss, while consistency is not obtained for the case of non-cavitation. An application is made on a real case of solid skirt piston of F8L413 Deutz Diesel engine currently mounted on TB260 trucks of SNVI company (currently DVP), Rouiba, in Algeria.

Received 11 February 2024; received in revised form 8 March 2024; accepted 14 August 2024.
To cite this article: Mohamed et al (2024). Cavitation modeling effect on tribological performances in piston skirt lubrication. JurnalTribologi 42, pp.198-215.

1.0 INTRODUCTION

In order to increase engine performance, interface between piston skirt and cylinder liner is the most investigated area toward reducing oil consumption, gas emission, noise and optimum tribological phenomena like wear, friction minimum film thickness and maximum pressure. Those parameters as well as the entire hydrodynamic pressure field influenced by the cavitation in the lubricant fluid film. The piston cylinder assembly represents 40 to 50% of power loss in an internal combustion engine (Comfort Allen 2004).

The cavitation is defined as a rapid formation and collapses of vapor bubbles in specific areas of the lubricant fluid (Letchford, 2016). The phenomenon occurs in the diverging region when local pressure drops below the atmospheric pressure, consequently, it reduces the load-carrying capacity of the interface and influences the lubricant film thickness as well as the friction force.

Cavitation modeling in electrohydrodynamic contact has been extensively investigated to identify the phenomenon that describes rupture and reformation of the lubricating fluid film.

Several models have been proposed such as Reynold, Gümbel (half-Sommerfeld), Jacobson Floberg Olsson and Elrod algorithm. Each model differs from the others by its specificity. Where Gümbel's model admit the discontinuity of the flow with the Negative pressure perceived as a sign of rupture of oil film (Gümbel, 1921) ,the conservation of mass is respected by Reynold's model by introducing the rupture of oil film without the reformation by dint of the conditions established by Swift (Swift, 1932) and (Stieber, 1933).

Olsson preceded by Jacobson and Floberg (Jacobson et al 1957) developed a theory (JFO) that ensures the conservation of mass and taking into account the rupture and the reformation of oil film.

Elrod (Elrod, 1981) proposed an algorithm that transformed the Reynold's equation into a mass conservation equation, which focuses on fluid density rather than pressure.

Other authors such as (Vijayaraghavan & Keith, 1989 ; Bayada et al., 1990 ; Kumar & Booker, 1991 ; Bonneau et al., 1995 ; Dowson et al., 1978) have further refined cavitation models, each tailored to specific well-defined conditions.

Several researches have examined the importance of cavitation consideration on the modeling of lubricated contacts. (Tauviqirrahman et al., 2016 ; Almaida et al., 2018) and (Rasep et al., 2021) showed that the cavitation must be taken into account in order to make more accurate predictions of the hydrodynamic pressure and the corresponding load-carrying capacity.

The piston-cylinder interaction area, or more precisely the radial clearance between the piston skirt and the cylinder liner is a critical region where the occurrence of cavitation is highly probable. This system can be represented by a set of surfaces lubricated by a thin film of oil (Shaw et al 1945.) .

In order to examine the cavitation in the lubrication of the piston, several algorithms have been developed such as (Yang & Keith, 1995 ; Sawicki & Yu, 2000) and recently (He et al., 2018)

The aim of this study is to develop a hydrodynamic lubrication model with Murty's algorithm (Murty, 1974) to determine the cavitation and its effect on the tribological parameters of lubricated piston-cylinder contacts.

2.0 METHODOLOGY

2.1 Mathematical Modeling of The Cavitation in Piston Cylinder

In hydrodynamic lubrication the piston skirt behavior is described simultaneously by a nonlinear second order system of two transient dynamic equations related to equilibrium of forces and moments about the wrist-pin and the Reynolds equation (Zhu et al., 1992 ; Abbes et al., 2012).

These equations are coupled by the eccentricities $e_t(t)$, $e_b(t)$ of the skirt in secondary movement, the velocity U in the axial movement and the pressure $p\ (x, y, t)$ of the oil lubricant film region located at major thrust side in the load bearing arc bounded by $(-\theta_1\ , \theta_1)$ named zone 1, and in the minor thrust side bounded by $(\pi - \theta_2,\ \ \pi + \ \theta_2)$ (figure. 1 a-b).

$$\begin{cases} \left[m_{pist}\left(1-\frac{b}{L}\right)+m_{pin}\left(1-\frac{a}{L}\right)\right]\ddot{e}_t+\left[m_{pist}\frac{b}{L}+m_{pin}\frac{a}{L}\right]\ddot{e}_b = F+\left(F_G+\bar{F}_{IP}+\bar{\mathrm{F}}_{\mathrm{IC}}+F_f\right)tg\phi \\ \left[\frac{I_{pist}}{L}+m_{pist}(a-b)\left(1-\frac{b}{L}\right)\right]\ddot{e}_t-\left[\frac{I_{pist}}{L}+m_{pist}(a-b)\left(\frac{b}{L}\right)\right]\ddot{e}_b = M+F_G C_P-\bar{F}_{IC}C_g+M_f \\ \frac{1}{R^2}\frac{\partial}{\partial\theta}\left(\frac{h^3}{\mu}\frac{\partial p}{\partial\theta}\right)+\frac{\partial}{\partial y}\left(\frac{h^3}{\mu}\frac{\partial p}{\partial y}\right)=U\frac{\partial h}{\partial y}+2\frac{\partial h}{\partial t} \end{cases} \tag{1}$$

Where R is the piston radius, ℓ the connecting-rod length, m_{pist} the piston mass, m_{pin} the wrist-pin mass, L the piston-skirt length, θ the circumferential coordinate fluid film of the skirt, C_p the wrist-pin offset, C_g the distance of the piston center of mass from the wrist-pin axis, μ the lubricant viscosity, a the piston axis position, b position of the center of mass piston, I_{pist} the piston inertia moment about its center of mass, F_G force due to combustion gas pressure, $(F_{IC}, \bar{F}_{IC})$ Inertia forces due to piston mass, $(F_{IP}, \bar{F}_{IP})$ inertia forces due to wrist-pin and connecting-rod small end mass, F load capacity of the hydrodynamic fluid film and M hydrodynamic moment about wrist-pin (Figure 1c).

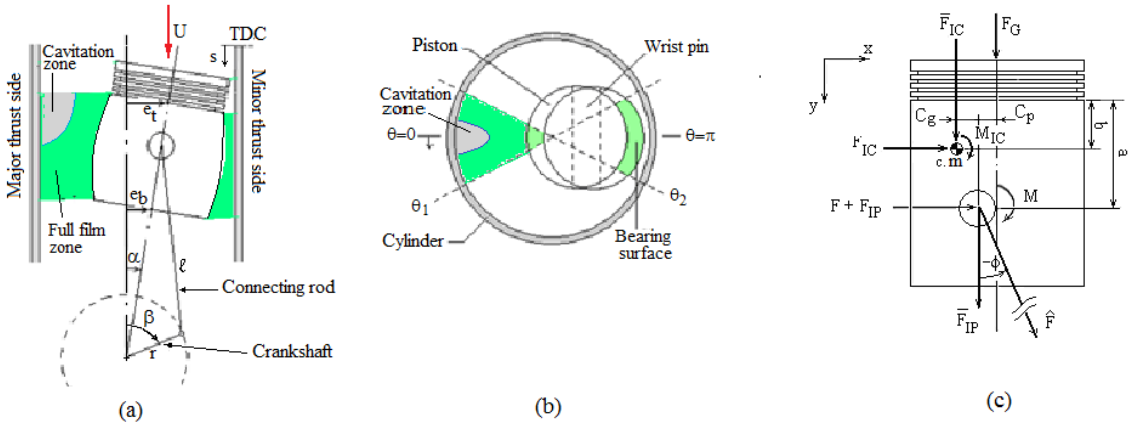

Figure 1: Schematic piston skirt-cylinder lubrication with cavitation.

Reynolds equation must be modified to take into account the cavitation in the lubricant fluid film. Cavitation, or partial lubrication, may occur when the local pressure in the oil film drops to

that of the oil vapor. The fluid film is unable to withstand the tension, resulting in its rupture. This may happen when the skirt is leaving the liner due to the piston motion, producing a diverging wedge. The rate of change of the film shape with respect to time $\partial h/\partial t$ and spatial coordinates ($\partial h/\partial y$, $\partial h/\partial \Theta$) increases so the term $U\,\partial h/\partial y + 2\,\partial h/\partial t$ increase, thus the functional becomes negative. (Bonneau & Hajjam, 2001):

$$f(p)=\frac{1}{R^2}\frac{\partial}{\partial\theta}\left(\frac{h^3}{\mu}\frac{\partial D}{\partial\theta}\right)+\frac{\partial}{\partial y}\left(\frac{h^3}{\mu}\frac{\partial p}{\partial y}\right)-U\frac{\partial h}{\partial y}-2\frac{\partial h}{\partial t}<0 \tag{2}$$

This lead to consider cavitation as a complementarity problem for searching the pressure P in the cavitation region as, either $f(p)<0$ and $p=0$ for cavitated zone or $f(p)=0$ and $p>0$ for active region. Instead of solving the complementarity problem by classical methods, which encounters challenges in ensuring flow continuity in cavitation regions, we utilize the universal cavitation algorithm based on the Jakobsson–Floberg–Olsson theory and revised by Elrod. The Elrod cavitation model avoids the tedious calculation of the cavitation boundary by reformulating the problem in terms of unique differential equation: A modified Reynolds equation, applicable to both the full film region and the cavitation region.

$$F\frac{1}{R^2}\frac{\partial}{\partial\theta}\left(\frac{h^3}{\mu}\frac{\partial D}{\partial\theta}\right)+F\frac{\partial}{\partial y}\left(\frac{h^3}{\mu}\frac{\partial p}{\partial y}\right)=U\frac{\partial h}{\partial y}+2\frac{\partial h}{\partial t}+(1-F)\left(U\frac{\partial D}{\partial y}+2\frac{\partial D}{\partial t}\right) \tag{3}$$

Where F is a switch function that takes the values: 1 in the full film region and 0 in a partial film region, D is a universal variable that replaces the film pressure p.

$$\begin{array}{llll} D=p, & F=1 & D\geq 0 & \text{in full film region} \\ D=h^*-h, & F=0 & D<0 & \text{in cavitation regions} \end{array} \tag{4}$$

where h^* is the filling ratio or the equivalent film thickness in cavitation region, given by

$$h^*=\alpha h \tag{5}$$

With $\alpha=\frac{\rho_c}{\rho_f}$ known as the fluid fraction content at the cavitation zone, is the ratio between the density of the full film (ρ_f) to the density of partial fluid in the cavitation zone (ρ_c).

Equation of the cavitation region is written as (*F=0* in equation (3))

$$U\frac{\partial h^*}{\partial y}+2\frac{\partial h^*}{\partial t}=0 \tag{6}$$

In active zones the transverse load-carrying capacity and moment about the wrist pin is expressed by

$$F=2\int_0^L\int_0^\pi p\cos\theta\, R d\theta dy \tag{7}$$

$$M=2\int_0^L\int_0^\pi p(a-y)\cos\theta\, R d\theta dy \tag{8}$$

The lubricant film thickness is given by

$$h = c + e_t cos\theta + \frac{y}{L}(e_t - e_b)cos\theta + s(y) \quad (9)$$

c is the nominal radial clearance between the piston and the cylinder bore, $s(y)$ is the piston skirt surface profile measured from the cylindrical reference surface.

The instantaneous viscous friction force in the lubricating film of the skirt is integrated over the surface S of the lubricated skirt by

$$f_c(t) = 2R\int_S \tau d\theta dy \quad (10)$$

Where τ is the shear stress in the lubricating film given by

$$\tau = \frac{h}{2}\frac{\partial p}{\partial y} - \alpha\frac{\mu U}{h} \quad (11)$$

The coefficient α is the fluid fraction defined by

$$\alpha = \frac{h^*}{h} = \frac{\rho_c}{\rho_f} \quad (12)$$

The instantaneous power loss at temps t is given at each time t by

$$P(t) = f_c(t)U(t) \quad (13)$$

$U(t)$ is the instantaneous axial velocity of the piston

2.2 Method for Solving Cavitation in Piston Cylinder

The non-linear system of differential equation (1).is solved by Newton–Raphson method. The numerical process is outlined in the following steps:

1. Reading data and initializing the unknown eccentricities $e_t(t)$ and $e_b(t)$.
2. for each engine cycle compute solution $e_t(t)$, $e_b(t)$,*p(x, y, t)* by the following steps.
   -for each crank angle (step time)
   -for each cavitation iteration until stability of the cavitation area (cavitation loop) by Murty modified algorithm
   -Use modified Newton-Raphson method to solve the non-linear system of differential equations (1) at i[th] iteration

$$\begin{Bmatrix} p \\ e_t \\ e_b \end{Bmatrix}^{(i+1)} = \begin{Bmatrix} p \\ e_t \\ e_b \end{Bmatrix}^{(i)} + \{y\}^{(i)} \quad (14)$$

Where $\{y\}^{(i)}$is the solution of the linear system $\{R\} + [J]\{y\} = 0$, $\{R\} = [E(p, e_t, e_b) \quad E_1(p, e_t, e_b) \quad E_2(p, e_t, e_b)]^T$ is the residual vector of equation (1), and $[J]$ the Jacobian matrix given by

$$[J]^{(i)} = \begin{bmatrix} \partial E/\partial p & \partial E/\partial e_t & \partial E/\partial e_b \\ \partial E_1/\partial p & \partial E_1/\partial e_t & \partial E_1/\partial e_b \\ \partial E_2/\partial p & \partial E_2/\partial e_t & \partial E_2/\partial e_b \end{bmatrix}^{(i)} \quad (15)$$

3. Continue to solve *p, h*, until residual vector reaches a value less than ε
4. Compute the equivalent film thickness h^* for the cavitation zone, the hydrodynamic loads *(F, M)* and the film thickness *h* of the lubricant film using respectively equations (5), (7-8) and (9)
5. Modify the boundary of the cavitation zone
6. Proceed for the next crank angle until achieved he actual cycle. Repeat the whole process for the next cycle until solution becomes cyclic i.e $e_t(\bar{t}) = e_t(\bar{t} + 4\pi)$ and $e_b(\bar{t}) = e_b(\bar{t} + 4\pi)$.

2.3 Finite Difference Grid for Solving Reynolds Equation

The Reynolds equation is solved by finite difference method. The lubricant fluid film of the piston skirt is modeled in 2D scheme by a rectangular finite difference grid (figure 2b) with $n_\theta \; x \; n_y$ points. Zones which contain wrist pin, defined by $[\theta_1 , \pi - \theta_2]$ and $[\pi + \theta_2 , 2\pi - \theta_1]$ are considered as inactive zones (Figure 2).

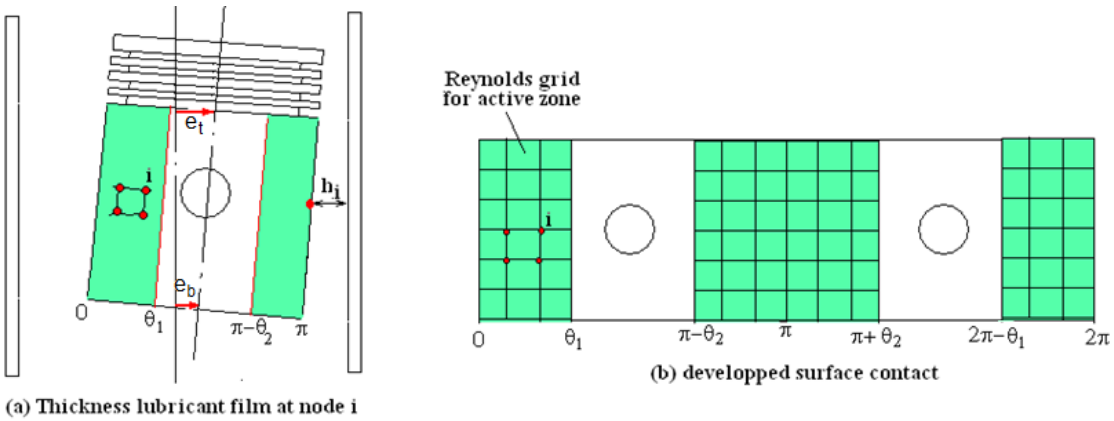

Figure 2: Grid of developed lubricant film.

2.4 Murty's Algorithm

To find the zone of cavitation as discussed above, we use Murty's algorithm.

1. We propose a cavitated zone Ω_c, *p=0* for all nodes
2. The Reynolds equation for pressure *p* in the active zone Ω is then solved
3. We verify the inequality (2) in Ω_c. Any node that does not satisfy this condition is positioned in Ω.
4. Node in Ω with a negative pressure *P* is placed in Ω_c. The pressure at this node is set to zero.

This procedure is repeated until stability of the cavitated zone is obtained

2.5 Resolution Method

The flowchart presented in figure 3 outlines the numerical method for solving the governing equations (1) for e_t, e_b, p taking into account cavitation in the lubricant film. The obtained solution must be a periodic ie which repeats itself at each engine cycle. In the set of nonlinear equations (1), the piston acceleration is computed by a numerical differentiation by using backward finite difference scheme.

$$\ddot{e}_t(t) = \frac{e_t(t) - 2e_t(t - dt) + e_t(t - 2dt)}{dt^2} \quad (16)$$

A similarly expression is written for $\ddot{e}_b(t)$. System (1) is now expressed only as a function of p, e_t and e_b and can be solved at each crank angle by the Newton-Raphson method. Starting from initial solution, the eccentricities $e_t(t - dt)$ and $e_t(t - 2dt)$ which appear in expression (16) are already known in the previous crank angle step. At each step, when using Newton-Raphson method, the linear system $\{R\} + [J]\{y\} = 0$ is solved for $\{y\}$ by numerically Cholevsky method and finally one can obtain $(p, e_t,\ e_b)$ by equation (14). In the run the combustion gas is introduced at each crank angle using the relation $F_G(t) = \frac{\pi D^2}{4} p_G(t)$ where pressure $p_G(t)$ is obtained from figure 5.

It is found from run, that 3 to 4 iterations of Newton–Raphson method are enough for the convergence of the solution with a precision $\varepsilon = 10^{-8}$ for the vector residue *{R}.* The determination of active and non-active areas is taken into consideration in the resolution using the Murty algorithm. In principle *ncavit* equal 2 to 5 iterations are enough to reach invariable and stable boundary. Once the solution is obtained the process is repeated for the next crank angle. Once the cycle is completed, the calculation is repeated for a second cycle until cyclic convergence is obtained. It is observed that converged solution is achieved within *ncycl* equal 3 to 4 engine cycles.

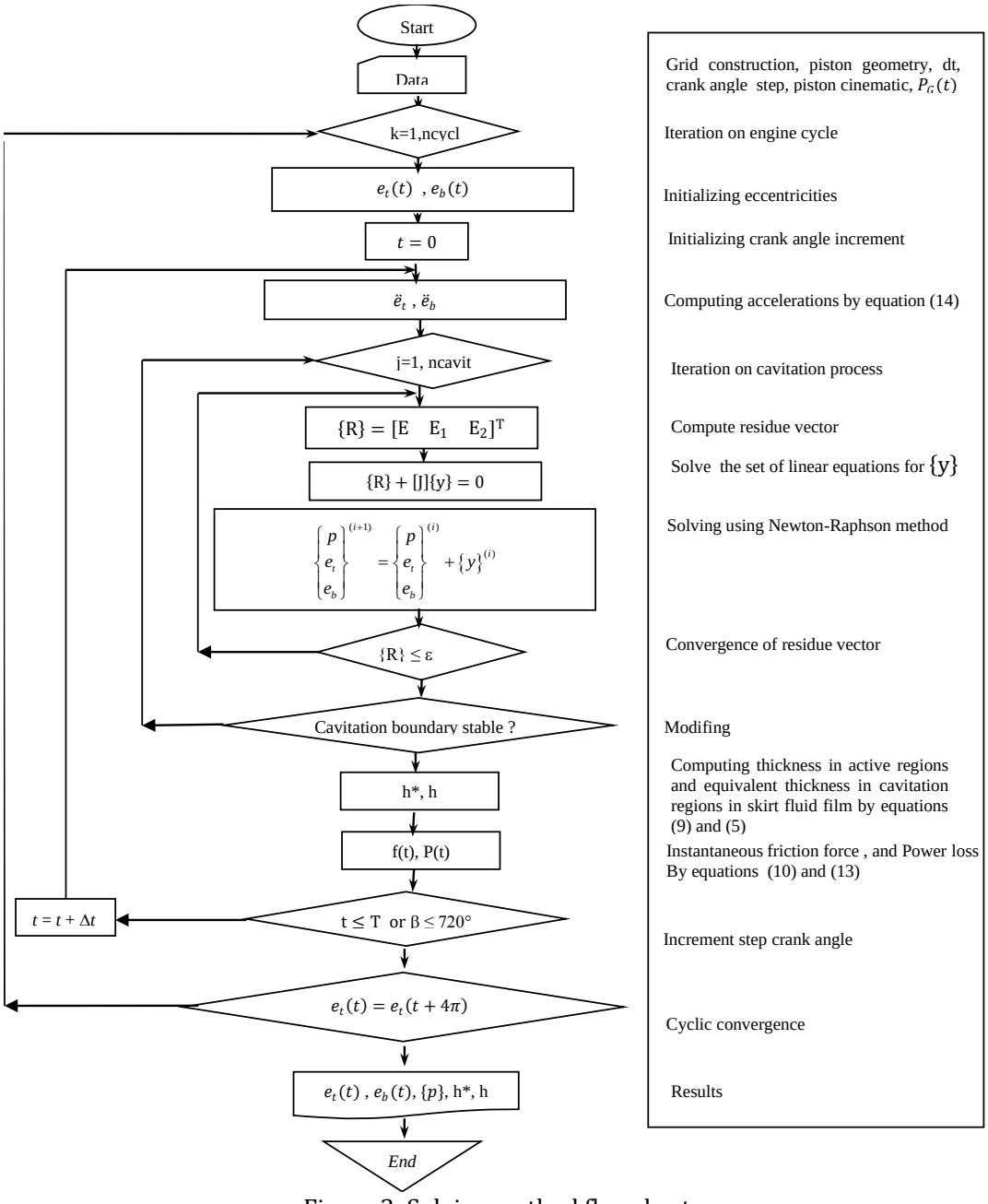

Figure 3: Solving method flowchart.

2.6 Mean Data of The Piston Model in Numerical Simulation

Numerical simulations have been conducted on a solid skirt piston of theV-8 diesel engine 'Deutz' F8L413 (Figure4) mounted currently on the TB230 trucks of the SNVI Rouiba in Algeria. The main engine parameters are listed in table 1:

Table 1: The main engine data.

Items	Specifications
Piston radius R	60 mm
Engine half stroke r	62.5 mm
Connecting-rod length (ℓ)	238 mm
Piston and connecting small end masses (m_{pist})	1.9 kg
Wrist-pin mass (m_{pin})	0.9 kg
Inertial moment of the piston	0.00066 Kgm^2
Nominal radial clearance (c)	0.035 mm
Piston-skirt length (L)	90 mm
Active pressure fluid film angle of the skirt (θ_1)	50 degrees
Wrist-pin offset pin (C_p)	0.0015 m
Distance of the piston center of mass from the wrist-pin axis (C_g)	0 mm
Crankshaft rotational speed (ω)	2000 rpm
Lubricant viscosity (μ)	0.0069 Pa.s
Piston axis position (a)	37 mm

(a) (b)

Figure 4: (a) V-8 diesel engine 'Deutz F8L413' and (b) the piston solid skirt.

3.0 RESULTS AND DISCUSSION

3.1 Dynamic Load

The combustion gas pressure acting on the piston head during one engine cycle versus crank angle of the crankshaft is plotted in figure 5. The curve is obtained by using specific thermodynamics and cinematic data of the actual Deutz engine F8L413. The cycle, a four-strokes engine completing two complete revolutions of the crankshaft, starts with intake stroke (0 - 180 deg crank angle) followed by a compression stroke (180-360 deg.); then by a combustion close to 360 deg resulting in a power stoke (360-540 deg), and finally exhaust stroke (540-720 deg). The diagram of figure 5 is obtained basically in two steps. First an actual P-V diagram of engine F8L413

is constructed by computing the pressure at each stroke by using analytical thermodynamics laws (Mariotte and Laplace law). A computer program is used to achieve this result. In a second step an indicated diagram is extracted from the above P-V diagram using graphically method to obtain the developed pressure as a function of the crank angle as shown in figure 5. The figure indicates that maximum pressure occurs after compression stroke at 372 deg crank angle, near the TDC (Top Dead center) where a value of 8.2 MPa is reached. In literature the results of he obtained diagram are specific to this Diesel engine type.

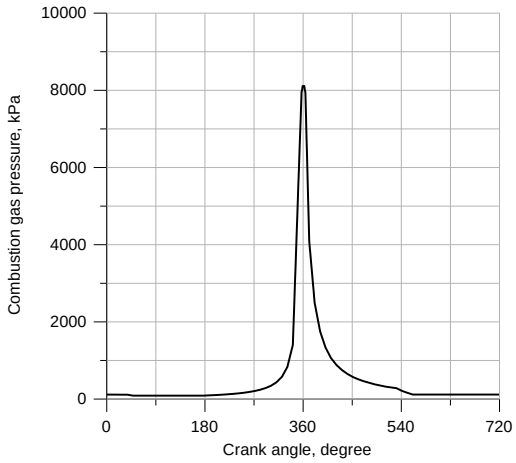

Figure 5: Combustion gas pressure on an engine cycle.

3.2 Effect on Pressure Distribution

Pressure distribution in the lubricant film $p(i,j)$ i.e. vector pressure $\{p\}$ is determined at each crank angle or step time by using Newton procedure (14) at each cavitation iteration of Murty algorithm according to the method flowchart presented in figure 3. For a fixed crank angle, the instantaneous maximum pressure is determined by the maximum value of the pressure distribution $p(i,j)$.

Figure 6 presents the comparison of Instantaneous maximum pressure for cavitation and without cavitation case as a function of crank angle with operating speed of 2000 rpm. The obtained results show that higher values are obtained when cavitation is not considered. In the power stroke a value of 7,757 MPa at 465° is reached for the non-cavitation case against 3,848 MPa at 395° for cavitation case. The pressure intensity is overestimated when cavitation is not considered.

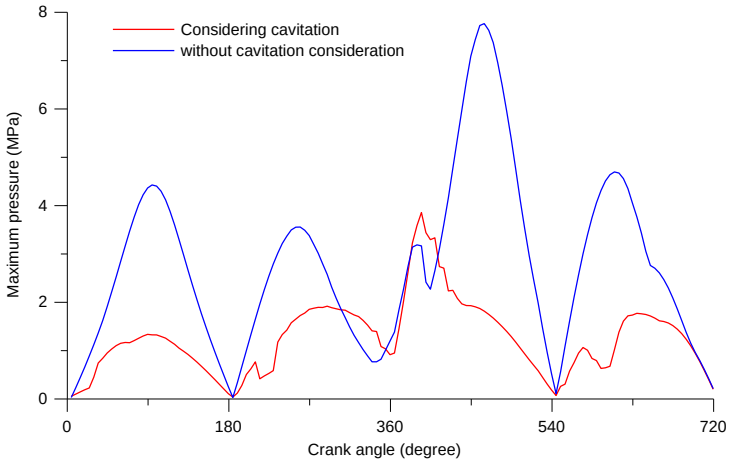

Figure 6: Comparison of Instantaneous maximum pressure for cavitation and without cavitation as a function of crank angle.

Analysis for specific crank angle. The large number of time steps leads us to consider only the effect of cavitation in severe conditions for specific crank angle of the piston movement.

We choose the crank angles for which the pressure is maximum in each engine stroke. Figure 6 which show that maximum pressure occurs at the middle of each engine stroke. We have $p_{max1} = 1.328$ MPa at $\beta = 90$ crank angle degree in intake stroke, $p_{max1} = 1.844$ MPa at $\beta = 270°$ in compression stroke, $p_{max1} = 3.848$ MPa at $\beta = 395°$ in power stroke and $p_{max1} = 1.762$ MPa at $\beta = 635° °$ in exhaust stroke.

The correspondent pressure distributions for the four-crank angle β case considering cavitation and non-cavitation are given in figure 7. Negative and positive pressure occurs in zone 1 $(-\theta_1 , \theta_1)$ or in zone 2 $(\pi - \theta_2, \pi + \theta_2)$ according to the crank angle when the non-cavitation or cavitation are respectively considered. This result validates the Reynolds and the Elrod cavitation models. Figure 7 also indicates that when the cavitation effect is considered, a significant difference between the two considerations is observed, where's, the predicted pressure is always smaller than that without cavitation for the four-crank angle.

The maximum pressures for critical values of crank angle are summarized in table 2. It can be concluded that the prediction of the lubrication behavior according to pressure distribution without considering cavitation is around 44 to 67 % larger than that with cavitation. This results for the present study are in agreement with the work presented by(Tauviqirrahman et al., 2016). Therefore, this shows the importance to take into account cavitation because it will have an impact on the piston behavior toward the maximum pressure of the lubricant and, will have an impact in evaluating the performance of the piston skirt lubrication.

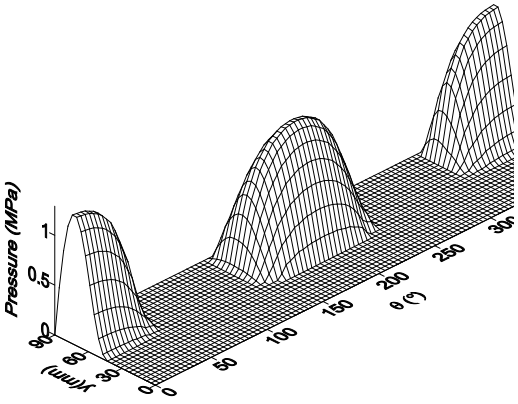

(a) With cavitation $\beta = 90°$

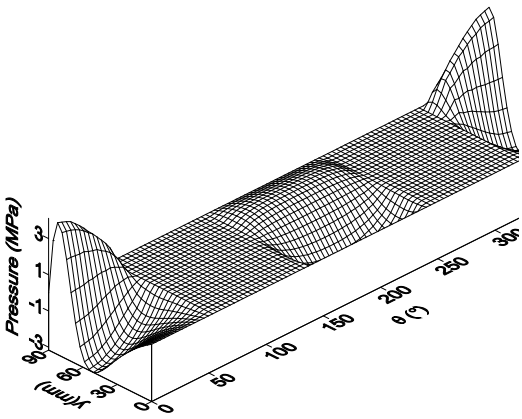

(b) Without cavitation $\beta = 90°$

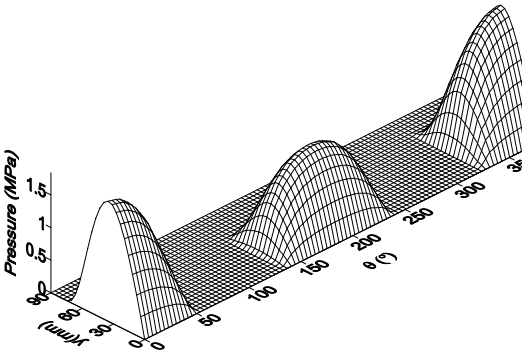

(c) With cavitation $\beta = 270°$

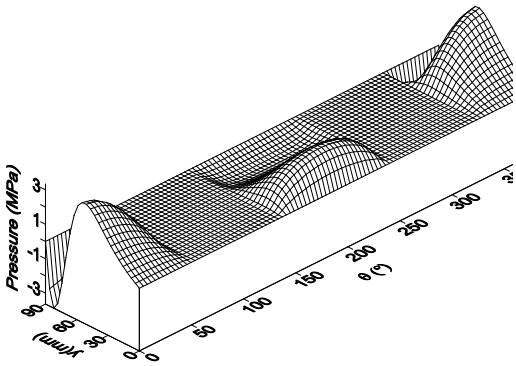

(d) Without cavitation $\beta = 270°$

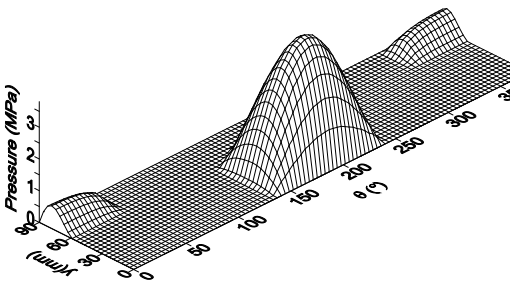

(e) With cavitation $\beta = 395°$

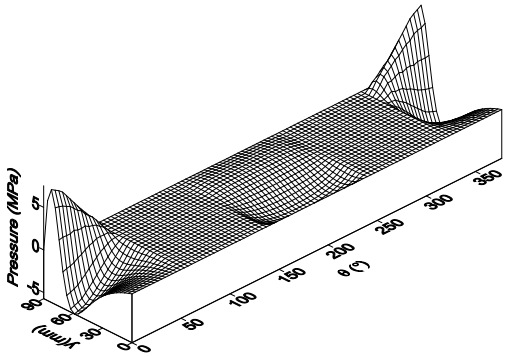

(f) Without cavitation $\beta = 465°$

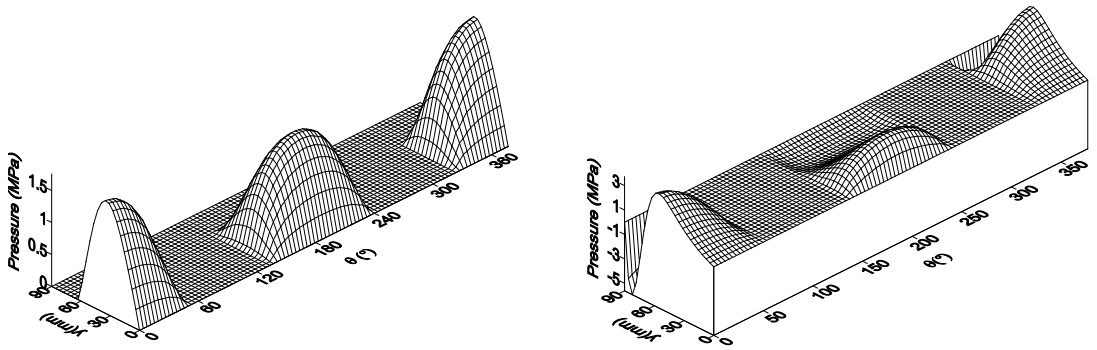

(g) With cavitation $\beta = 635°$ (h) Without cavitation $\beta = 635°$

Figure 7: Oil film pressure distributions for cavitation and without cavitation for critical crank angle.

Table 2: Performance of maximum pressure in case of cavitation and non-cavitation.

Crank angle β (°)	With cavitation	Without cavitation	Difference (%)
90	1.323	4.123	67
270	1.844	3.341	44
395	3.848	7.757	50
635	1.762	3.744	53

3.3 Effect on The Eccentricity at The Top and Bottom of Skirt

The eccentricities $e_t(t)$,and $e_b(t)$ are obtained by the numerical method presented in the flowchart of figure 3, detailed in section 2.5. The Jacobian matrix and the residue vector which appear in the calculation of the eccentricities in Newton method contain the geometry data of the piston and the simulation parameters according to table 1.

A computer program written in Fortran is developed to obtain the eccentricities at each crank angle iteration according to the flowchart of figure 3.

Figure 8 gives the piston eccentricities $e_t(t)$ and $e_b(t)$ versus crank angle considering both cavitation and non-cavitation. When cavitation is considered, the upper skirt piston (figure 8a) performs a lateral oscillatory movement toward the minor thrust side (positive eccentricities) during the entire cycle. The top eccentricity reaches a maximum value of $e_t = 16.56\ \mu m$ at 425° after TDC in power stroke, the correspondent bottom eccentricity is $e_b = -14.712\ \mu m$. The piston position in this configuration is given in figure 9a.

It's clear that with configuration ($e_t = 4.674\ \mu m$, $e_b = -3.211\ \mu m$) the piston top moves toward minor thrust side and pressure must acts in zone 2 and with negative eccentricity the piston bottom moves toward major thrust side and pressure must acts in zone 1 (figure 9b). Or the obtained results of pressure distribution showed in figure 9b, that the results of pressure and eccentricities are consistent which validates the model with cavitation.

When cavitation is not considered, the piston movement obtained differs from the configuration validated above, the movement is too amplified in case of top eccentricity where a maximum of 30.14 μm at 720° in exhaust stroke is obtained. For bottom eccentricity the movement is located under the curve with cavitation during the entire cycle with a configuration not corresponding to the behavior of the piston obtained in the case of considering cavitation. It

becomes evident that there is a significant difference between the two curves; model without cavitation for eccentricities is not consistent for piston behavior.

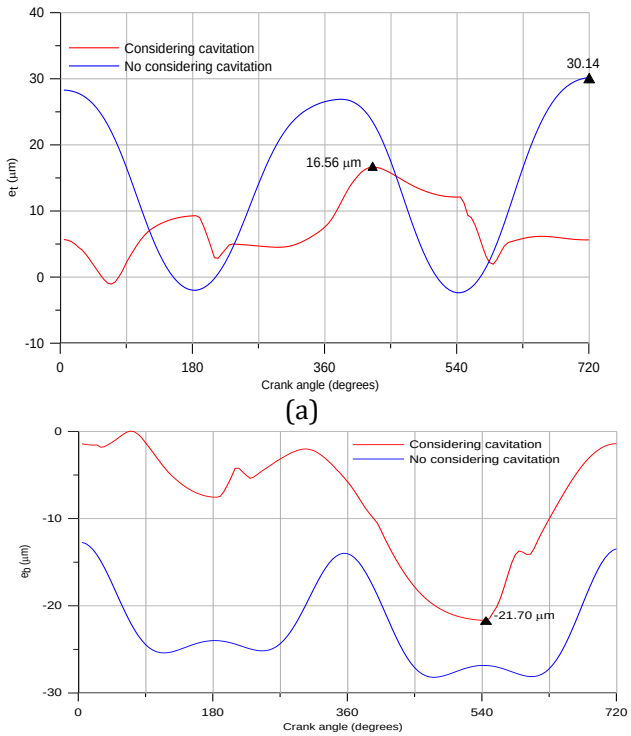

Figure 8: Comparison of eccentricities for the cavitation and no cavitation effect (a) top eccentricity of the skirt;(b) bottom eccentricity.

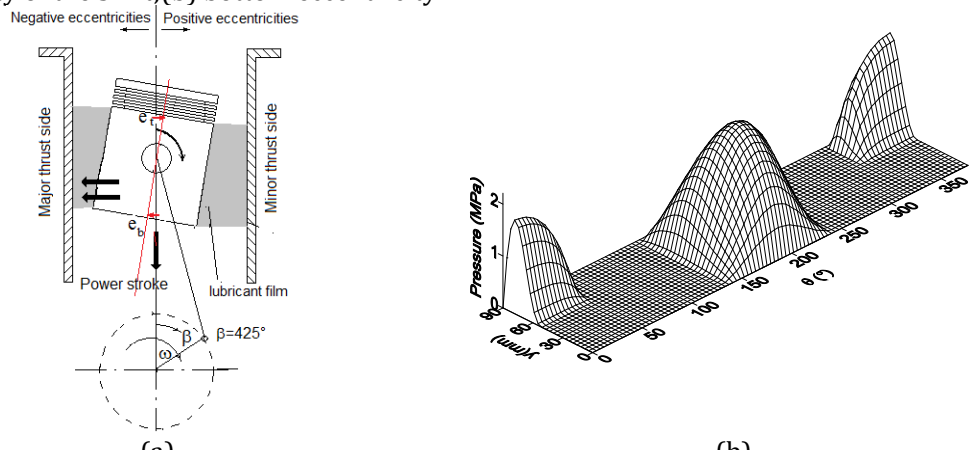

Figure 9: (a) Piston configuration at maximum top eccentricity and the correspondent bottom eccentricity at $\beta = 425°$ $e_t = 16.56$ µm , $e_b = -14.712$ µm and (b) pressure distribution for the correspondent configuration at $\beta = 425°$.

3.4 Effect on Minimum Oil Film Thickness

The thickness film h in active zone is obtained by equation (9), as function of the eccentricities $e_t(t)$ and $e_b(t)$ given by figure 8. The minimum film thickness h_{min} is calculated as the minimum value of the thickness film *h(i, j)* at each grid point.

Figure 10 shows the minimum lubricant film thickness at each crank angle, with and without cavitation. It shows that the minimum thickness with cavitation consideration varies slightly between 22 μm and 24 μm during the intake and compression stroke, followed by a significant decrease immediately after TDC in power stroke until reaching a minimum value of 11.935 μm at 545 crank angle deg. This result is in consistence with the other parameters.

On the other hand, the minimum thickness obtained in the case of without cavitation presents itself with peaks in each engine stroke without decreasing in the power stroke. These results show that the minimum film thickness is not consistent with the secondary movement of the piston when considering no cavitation effect.

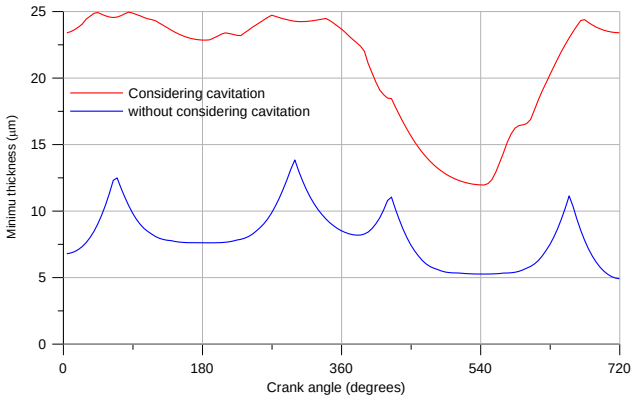

Figure 10: Comparison of minimum film thickness in the cases of cavitation and without consideration.

3.5 Effect on Friction and Power Loss

Once the distribution pressure determinate at each grid points of the lubricant film as detailed in section 3.2 for both cavitation and non-cavitation, viscous friction force in the skirt lubricant is computed from equation (10) at each crank angle step for all the engine cycle by using the computer program of the flowchart (figure 3). Figure 11 illustrates the friction force as a function of the crank angle for both case of cavitation and without cavitation. The two curves are of the same shape but have different amplitudes, the curve obtained for the case without cavitation is more amplified. This shows again the need to take into account the effect of cavitation to obtain more precise results.

The corresponding instantaneous power loss is calculated as a function of crank angle, for both cavitation and non-cavitation, by equation (13) are presented in figure 12. During power stroke after TDC, the power friction is maximum resulting from higher pressure in this piston position This results for the present study are in agreement with the work presented by (Li et al., 1983).

The instantaneous power loss and the friction force for critical values are summarized in table 3. It can be concluded that the prediction of the instantaneous power loss and the friction force when considering non-cavitation is around 15 to 19 % larger than that with cavitation. Therefore, it can be concluded that the cavitation model must be taken into account in lubrication analysis

because it will have significant effect on the result of the friction and the power lost by friction and, consequently on performance evaluation of the piston hydrodynamic lubrication.

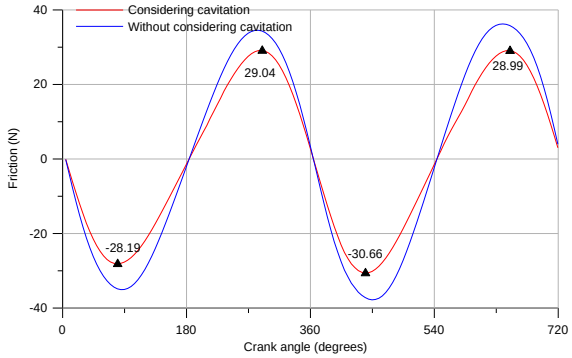

Figure 11: Instantaneous skirt friction for both cavitation and non-cavitation.

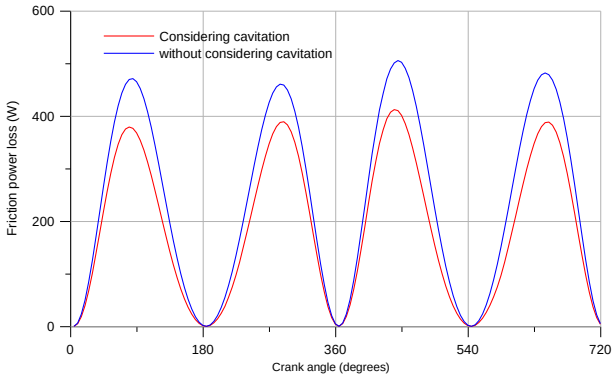

Figure 12: instantaneous friction power loss for both cavitation and non-cavitation.

Table 3: Performance of maximum Power loss and friction load at engine stroke in case of cavitation and non-cavitation.

Stroke	**Maximum Power loss (W)**			**Friction load (N)**		
	Cavitation	**Non-cavitation**	**Difference (%)**	**Cavitation**	**Non-cavitation**	**Difference (%)**
Intake	378.3	471.0	19.6	-28.19	-35.1	19.9
Compression	388.9	460.4	15.5	28.9	34.4	15.9
Power	412.1	505.3	18.4	-30.6	-37.8	19
Exhaust	388.3	481.8	19.4	28.9	36.4	20.6

CONCLUSIONS

A hydrodynamic lubrication model of engine piston skirt is analyzed in the case of cavitation and no cavitation effect on tribological parameters of the lubricant fluid film and on the piston secondary movement. The results are summarized as follows:

a. The comparison between the two cases shows that the predicted hydrodynamic pressure obtained in the case of non-cavitation is always higher, around 44 to 67 %, than that with the cavitation effect.
b. The results indicate that the cavitation effect gives a consistency between the secondary movement and the pressure distribution in the lubricant film while on the case of non-cavitation there is nonconsistency between the eccentricities and the pressure distribution. These results show also the minimum film thickness is not consistent with the secondary movement of the piston when considering no cavitation effect.
c. The results show that the prediction of the instantaneous power loss and the friction force when considering non-cavitation is around 15 to 19 % larger than that with cavitation.
d. The cavitation model must be taken into account in lubrication analysis because it will have significant effect on the result of the pressure, the secondary movement, and the tribological parameters and, consequently on the performance evaluation of the piston hydrodynamic lubrication.

REFERENCES

Abbes, M. T., Maspeyrot, P., Dekkiche, A., Benbrik, M., & Hacène, F. B. (2012). Elastohydrodynamic Piston Skirt Lubrication : Effect on Tribological Performances. International Joint Tribology Conference, 45080, 237-242.

Almaida, N., Prasetyaji, M. R., Mufian, M. H., Hakim, A. R., & Tauviqirrahman, M. (2018). Cavitation modelling effect on pressure distribution of inclined lubricated contacts and textured surfaces using CFD. Journal Tribologi, 22, 40-48.

Bayada, G., Chambat, M., & Elalaoui, M. (1990). Mathematical models and related algorithms in cavitation problems. Current research in cavitating fluid films, Part II: theoretical modelling ….

Bonneau, D., Guines, D., Freˆne, J., & Toplosky, J. (1995). EHD Analysis, Including Structural Inertia Effects and a Mass-Conserving Cavitation Model. Journal of Tribology, 117(3), 540-547. https://doi.org/10.1115/1.2831288

Bonneau, D., & Hajjam, M. (2001). Modélisation de la rupture et de la reformation des films lubrifiants dans les contacts élastohydrodynamiques. European Journal of Computational Mechanics, 679-704.

Dowson, D., Higginson, G. R., & Nielsen, K. W. (1978). Elasto-Hydrodynamic Lubrication (International Series in Material, Science and Technology, Vol. 23).

Elrod, H. G. (1981). A cavitation algorithm. https://citeseerx.ist.psu.edu/document?repid=rep1&type=pdf&doi=5ee02b2e81e122d8063ca0b828dafb268ebe9cf0

Gümbel, L. (1921). Verleich der Ergebnisse der rechnerischen Behandlung des Lagerschmierungsproblem mit neueren Versuchsergebnissen. Mbl. Berl. Bez.(VDI), 125-128.

He, Z., Gong, W., Xie, W., Zhang, G., & Hong, Z. (2018). A mass-conserving algorithm for piston ring dynamical lubrication problems with cavitation. Industrial Lubrication and Tribology, 70(1), 212-229.

Kumar, A., & Booker, J. F. (1991). A finite element cavitation algorithm : Application/validation.
Letchford, N. (2016). Cavitation in lubricating films [PhD Thesis, University of Oxford]. https://ora.ox.ac.uk/objects/uuid:17a49106-bb6d-443c-be6b-50398bbd4590
Li, D. F., Rohde, S. M., & Ezzat, H. A. (1983). An Automotive Piston Lubrication Model. A S L E Transactions, 26(2), 151-160. https://doi.org/10.1080/05698198308981489
Murty, K. G. (1974). Note on a Bard-type scheme for solving the complementarity problem. Opsearch, 11(2-3), 123-130.
Rasep, Z., Yazid, M., & Samion, S. (2021). A study of cavitation effect in a journal bearing using CFD : A case study of engine oil, palm oil and water. Jurnal Tribologi, 28, 48-62.
Sawicki, J. T., & Yu, B. (2000). Analytical Solution of Piston Ring Lubrication Using Mass Conserving Cavitation Algorithm. Tribology Transactions, 43(3), 419-426. https://doi.org/10.1080/10402000008982358
Shaw, M. C., & Nussdorfer, J. T. (s. d.). A visual and photographic study of cylinder lubrication. National Advisory Committee for Aeronautics. Report.
Stieber, W. (1933). Das schwimmlager : Hydrodynamische theorie des gleitlagers. (No Title). https://cir.nii.ac.jp/crid/1130282271232120704
Swift, H. W. (1932). THE STABILITY OF LUBRICATING FILMS IN JOURNAL BEARINGS. (INCLUDES APPENDIX). Minutes of the Proceedings of the Institution of Civil Engineers, 233(1932), 267-288. https://doi.org/10.1680/imotp.1932.13239
Tauviqirrahman, M., Muthik, B., Muchammad, M., Pratomo, A. W., & Jamari, J. (2016). Effect of cavitation modelling on the prediction of the lubrication performance using CFD : A case study of journal bearing lubricated with non-newtonian. http://doc-pak.undip.ac.id/812/1/peer_c4_tauviqirrahman.pdf
Vijayaraghavan, D., & Keith, T. G. (1989). Development and Evaluation of a Cavitation Algorithm. Tribology Transactions, 32(2), 225-233. https://doi.org/10.1080/10402008908981882
Yang, Q., & Keith, T. G. (1995). An Elastohydrodynamic Cavitation Algorithm for Piston Ring Lubrication. Tribology Transactions, 38(1), 97-107. https://doi.org/10.1080/10402009508983385
Zhu, D., Cheng, H. S., Arai, T., & Hamai, K. (1992). A Numerical Analysis for Piston Skirts in Mixed Lubrication—Part I : Basic Modeling. Journal of Tribology, 114(3), 553-562. https://doi.org/10.1115/1.2920917